Supporting Information

New Cu(I) halide complexes showing TADF combined with room temperature phosphorescence: the balance tuned by halogens

Andrey Yu. Baranov,[a] Alexey S. Berezin,[a] Denis G. Samsonenko,[a] Anton S. Mazur,[b] Peter M. Tolstoy,[b] Viktor F. Plyusnin,[c,d] Ilya E. Kolesnikov,[e] Alexander V. Artem'ev*[a]

[a] *Nikolaev Institute of Inorganic Chemistry, 3, Acad. Lavrentiev Ave., Novosibirsk 630090, Russian Federation*
[b] *Institute of Chemistry, St. Petersburg State University, Russian Federation*
[c] *Voevodsky Institute of Chemical Kinetics and Combustion, Institutskaya str. 3, 630090 Novosibirsk, Russian Federation*
[d] *Novosibirsk State University (National Research University), 2, Pirogova Str., Novosibirsk 630090, Russian Federation*
[e] *Center for Optical and Laser Materials Research, Saint Petersburg State University, Ulianovskaya, 5, Saint Petersburg 198504, Russian Federation*

*Author for correspondence: chemisufarm@yandex.ru (Alexander V. Artem'ev)

Table of Contents

§1. Experimental details

General remarks

CuI (99%, Sigma) and MeCN (HPLC grade, Cryochrom) were used as received. CuBr was freshly synthesized by treatment of $CuBr_2$ with Cu powder in MeCN solution. CuCl (≥99%, Sigma), prior to use, was additionally purified by subsequent washing with HCl_{aq}, water and acetone, followed by drying under vacuum. Tris(2-pyridyl)phosphine (Py_3P) was prepared following known procedure.[1]

XRPD analyses were performed on a Shimadzu XRD-7000 diffractometer (Cu-Kα radiation, Ni – filter, 3–35° 2ϑ range, 0.03° 2ϑ step, 5s per point). FT-IR spectra were collected on a Bruker Vertex 80 spectrometer. The microanalyses were carried out on a MICRO cube analyzer. Thermogravimetric analyses were performed in a closed Al_2O_3 pan under helium flow at 10 °C/min^{-1} heating rate using a Netzsch STA 449 F1 Jupiter STA.

Solid state NMR spectroscopy

The ^{13}C, ^{15}N and ^{31}P NMR spectra of **1** were measured using Bruker Avance III 400WB NMR spectrometer (161.976 MHz for ^{31}P; 100.613 MHz for ^{13}C; 40.56 MHz for ^{15}N) equipped with a magic angle spinning (MAS) probe. The samples were placed into 4 mm zirconia rotors and spun at 14 kHz. All CP (cross-polarization) MAS spectra were recorded with broadband ^{1}H decoupling at 25°C using the following delay times, contact times and the number of scans: 10 s, 0.5 ms and 1024 for ^{13}C; 3 s, 10 ms and 56000 for ^{15}N; 2 s, 2 ms and 1024 for ^{31}P. The chemical shifts are reported in the following scales: tetramethylsilane (TMS) for ^{1}H, liquid NH_3 for ^{15}N (recalibrated from NH_4Cl scale[2]) and 85% solution of H_3PO_4 in H_2O for ^{31}P.

Photophysical measurements

Excitation and emission spectra were recorded on a Fluorolog 3 spectrometer (Horiba Jobin Yvon) with a cooled PC177CE-010 photon detection module equipped with an R2658 photomultiplier. The luminescence decays and delayed luminescence spectra were measured on the same instrument. The absolute values of PLQYs were recorded using a Fluorolog 3 Quanta-phi device. The luminescence quantum yield at 77 K was obtained relative to the quantum yield of the same sample at 300 K. Independently, these relative quantum yields were calibrated by use of the absolute Φ_{PL} values measured at 77 K. Temperature dependences of luminescence were carried out using Optistat DN optical cryostats (Oxford Instruments).

The solid-state reflectance spectra were recorded on a Shimadzu UV-3101 spectrophotometer. Samples were prepared by a thorough grinding of a mixture of a complex (*ca.* 2 mol%) with $BaSO_4$. The reflectance data were converted into a spectrum applying a Kubelka-Munk function using $BaSO_4$ as a standard.

§2. Synthesis and characterization data

General procedures for synthesis of complexes 1–3

Synthesis in solution. To a mixture of tris(2-pyridyl)phosphine (62 mg, 0.23 mmol) and CuCl or CuBr (0.23 mmol), MeCN (4 mL) was added and the mixture was stirred at ambient temperature for 5 h. The precipitated powder was centrifuged and dried in air to give complex **1** or **2** in 90–95% yield. The iodide complex **3** was prepared by a similar way using 20% excess of CuI, i.e. 0.27 mmol.

Solvent-assistant mechanochemical synthesis. Tris(2-pyridyl)phosphine (106 mg, 0.40 mmol), Cu(I) halide (0.40 mmol) and several drops of MeCN (~0.2 mL) were placed to an agate mortar. The mixture was ground with a pestle for a minute. The resulting off-white solid was washed with small amount of MeCN to afford corresponding complex in about 99% yield.

*$[Cu_2(Py_3P)_2Cl_2]$ (**1**)*
Off-white powder. *Anal*. Calc. for $C_{30}H_{24}Cl_2Cu_2N_6P_2$ (728.50): C, 49.5; H, 3.3; N, 11.5%. Found: C, 49.6; H, 3.3; N, 11.4%. FT-IR (KBr, cm^{-1}): 432 (m), 482 (vs), 534 (vs), 637 (w), 725 (m), 746 (m), 768 (s), 783 (s), 797 (m), 984 (m), 1009 (m), 1047 (m), 1086 (m), 1157 (m), 1236 (w), 1277 (w), 1292 (w), 1418 (s), 1423 (s), 1431 (s), 1452 (vs), 1560 (s), 1580 (vs), 2957 (w), 2980 (m), 3036 (m).

*$[Cu_2(Py_3P)_2Br_2]$ (**2**)*
Off-white powder. *Anal*. Calc. for $C_{30}H_{24}Br_2Cu_2N_6P_2$ (728.50): C, 44.1; H, 3.0; N, 10.3. Found: C, 42.2; H, 2.9; N, 10.1%. FT-IR (KBr, cm^{-1}): 432 (m), 480 (vs), 532 (vs), 637 (w), 746 (m), 768 (s), 779 (vs), 988 (m), 1009 (m), 1049 (m), 1086 (m), 1155 (m), 1420 (s), 1429 (s), 1452 (vs), 1560 (s), 1578 (vs), 3034 (m), 3061 (m).

*$[Cu_2(Py_3P)_2I_2]$ (**3**)*
Off-white powder. *Anal*. Calc. for $C_{30}H_{24}I_2Cu_2N_6P_2$ (728.50): C, 39.5; H, 2.6; N, 9.2. Found: C, 39.6; H, 2.5; N, 9.3%. FT-IR (KBr, cm^{-1}): 426 (w), 480 (s), 509 (m), 530 (s), 745 (m), 760 (s), 772 (s), 785 (m), 988 (m), 1007 (m), 1051 (w), 1153 (m), 1288 (w), 1412 (m), 1422 (s), 1452 (vs), 1560 (s), 1580 (s), 3038 (m).

§3. X-Ray crystallography

Single crystals of **1**–**3** were grown by vapor diffusion of diethyl ether into a CH_2Cl_2 solution at room temperature for a week. Diffraction data were obtained on an automated Agilent Xcalibur diffractometer equipped with an area AtlasS2 detector (graphite monochromator, λ(MoKα) = 0.71073 Å, ω-scans). Integration, absorption correction, and determination of unit cell parameters were performed using the CrysAlisPro program package.[3] The structures were solved by dual space algorithm (SHELXT[4]) and refined by the full-matrix least squares technique (SHELXL[5]) in the anisotropic approximation (except hydrogen atoms). Positions of hydrogen atoms were calculated geometrically and refined in the riding model.

The crystallographic data and details of the structure refinements are summarized in Table S1. CCDC 1960446–1960449 contain the supplementary crystallographic data for this paper. These data can be obtained free of charge from The Cambridge Crystallographic Data Center at http://www.ccdc.cam.ac.uk/data_request/cif.

Table S1. Crystal data and structure refinement for **1**–**3**.

	1	**2**	**3** (130 K)	**3** (295 K)
CCDC number	1960448	1960449	1960446	1960447
Chemical formula	$C_{30}H_{24}Cl_2Cu_2N_6P_2$	$C_{30}H_{24}Br_2Cu_2N_6P_2$	$C_{30}H_{24}Cu_2I_2N_6P_2$	$C_{30}H_{24}Cu_2I_2N_6P_2$
M_r	728.47	817.39	911.37	911.37
Crystal system, space group	Monoclinic, $P2_1/n$	Monoclinic, $P2_1/n$	Monoclinic, $P2_1/c$	Monoclinic, $P2_1/c$
Temperature (K)	130	100	130	295
a, b, c (Å)	8.7081(2), 11.8728(2), 14.9438(4)	8.7440(17), 11.9700(6), 15.2500(11)	9.2965(3), 11.2423(3), 15.8411(5)	9.3613(3), 11.3294(4), 15.9037(5)
α, β, γ (°)	103.577(2)	103.73(3)	103.457(3)	103.734(3)
V (Å^3)	1501.86(6)	1550.6(4)	1610.16(9)	1638.49(10)
Z	2	2	2	2
μ (mm^{-1})	1.73	5.48	3.37	3.31
Crystal size (mm)	0.35 × 0.09 × 0.07	0.10 × 0.03 × 0.03	0.12 × 0.07 × 0.04	0.16 × 0.07 × 0.06
T_{min}, T_{max}	0.968, 1.000	0.782, 1.000	0.971, 1.000	0.967, 1.000
No. of measured, independent and observed [$I > 2\sigma(I)$] reflections	10770, 3559, 3185	12373, 3426, 2764	7269, 3509, 3009	6707, 3197, 2733
R_{int}	0.022	0.052	0.021	0.018
$(\sin\theta/\lambda)_{max}$ (Å^{-1})	0.679	0.648	0.677	0.617
$R[F^2 > 2\sigma(F^2)]$, $wR(F^2)$, S	0.025, 0.065, 1.04	0.045, 0.122, 1.07	0.024, 0.048, 1.02	0.025, 0.055, 1.03
No. of reflections	3559	3426	3509	3197
No. of parameters	190	191	190	190
$\Delta\rangle_{max}$, $\Delta\rangle_{min}$ (e Å^{-3})	0.43, –0.38	1.05, –0.90	0.57, –0.43	0.61, –0.36

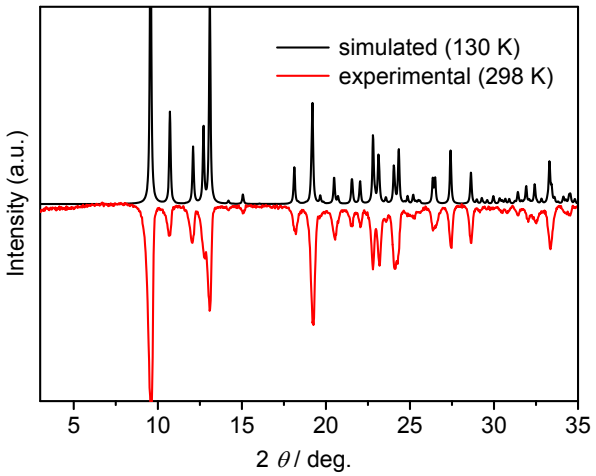

Figure S1. Experimental and simulated XRPD patterns for "as-synthesized" sample of **1**.

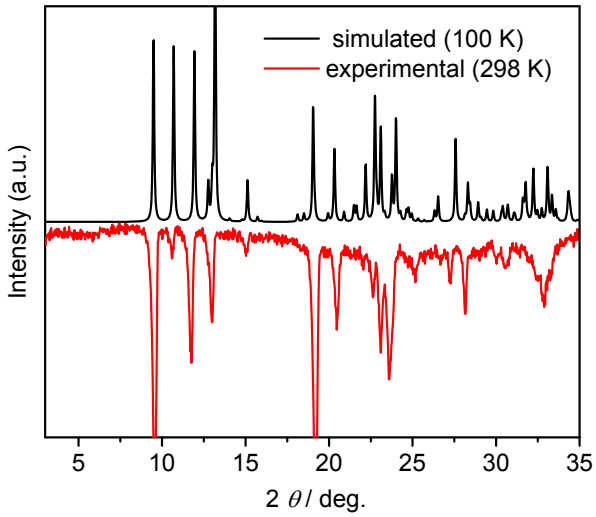

Figure S2. Experimental and simulated XRPD patterns for "as-synthesized" sample of **2**.

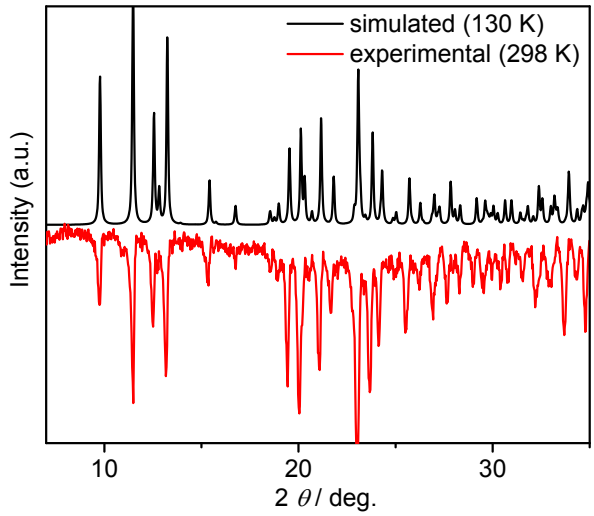

Figure S3. Experimental and simulated XRPD patterns for "as-synthesized" sample of **3**.

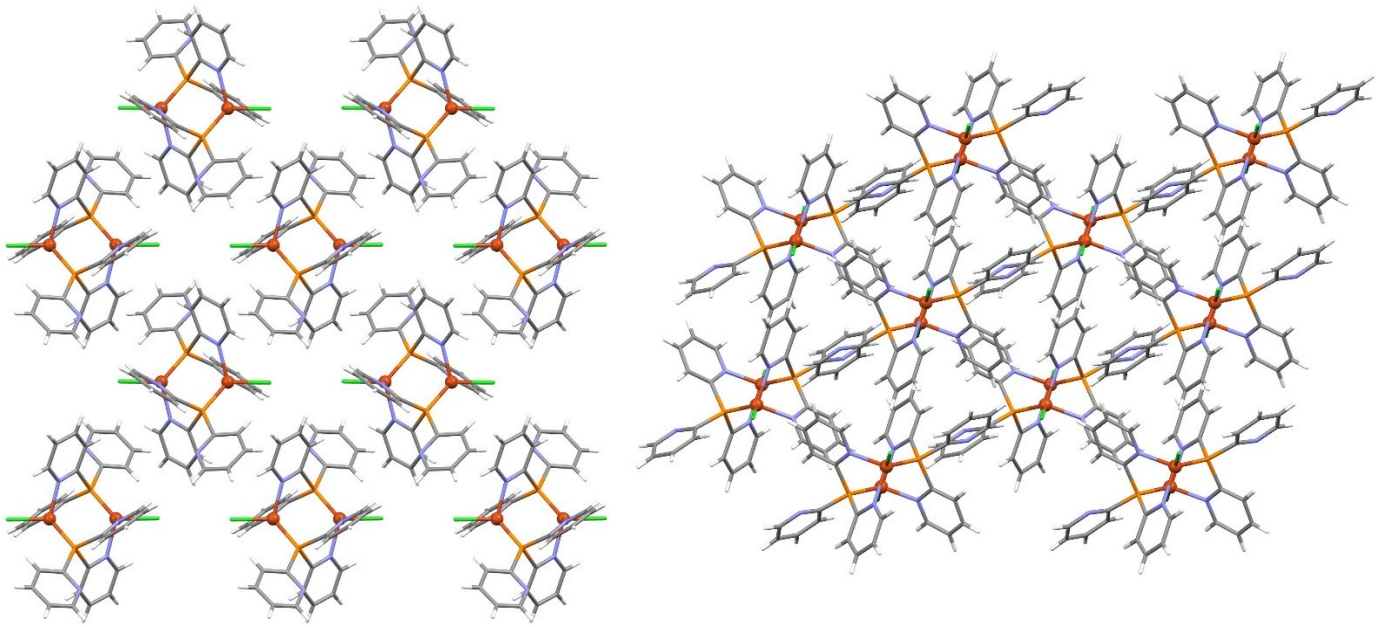

Figure S4. Crystal packing of **1** viewed along *a* (left) and *b* (right) axes.

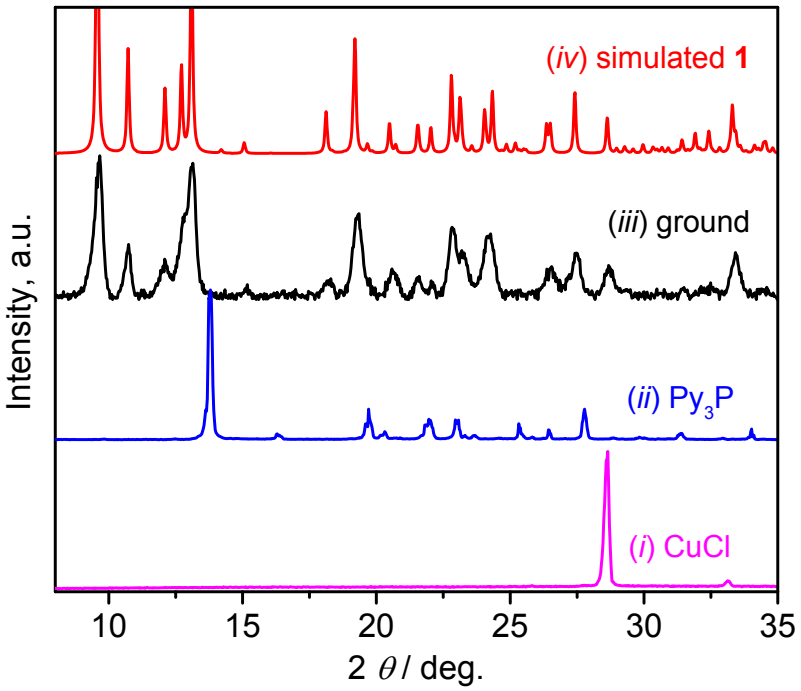

Figure S5. Change in PXRD patterns of the reactants during mechanosynthesis of **1**: (*i*) CuCl; (*ii*) Py_3P ligand; (*iii*) ground mixture (in presence of MeCN drops); (*iv*) simulated PXRD pattern for **1**.

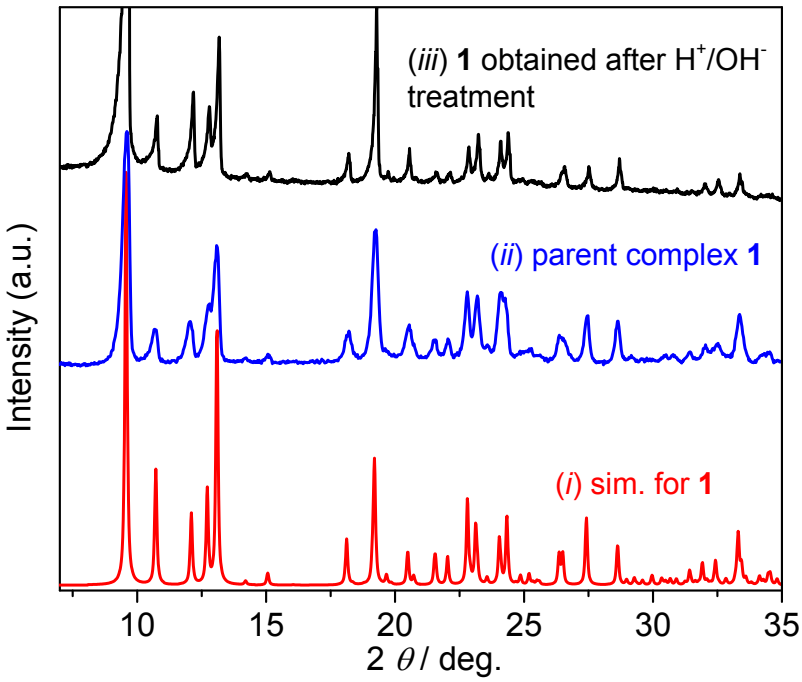

Figure S6. The PXRD patterns for complex **1**: (*i*) simulated one; (*ii*) obtained from Py_3P and CuCl *via* mechanochemical synthesis; (*iii*) precipitated by adding of $NaOH_{(aq)}$ to a solution of sample "*ii*" in aqueous HCl.

§4. FT-IR spectra

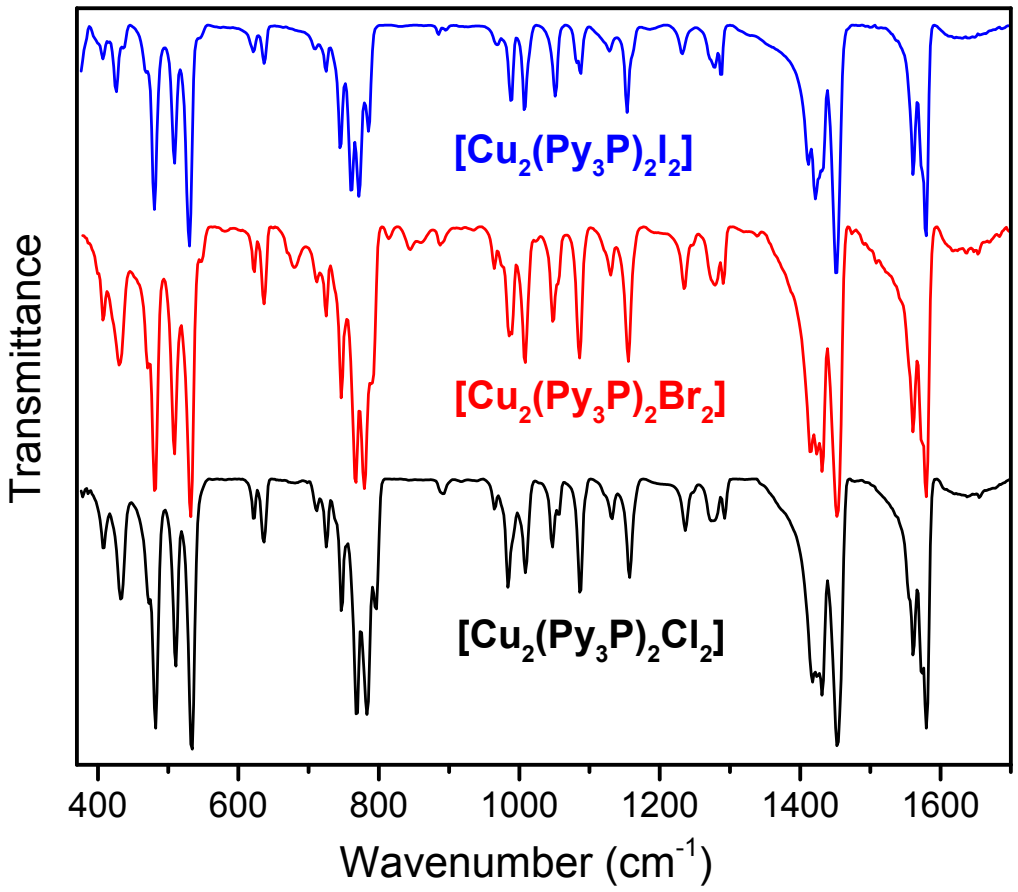

Figure S7. FT-IR spectra of complexes **1**–**3** in the fingerprint region.

§5. TGA&DTG curves

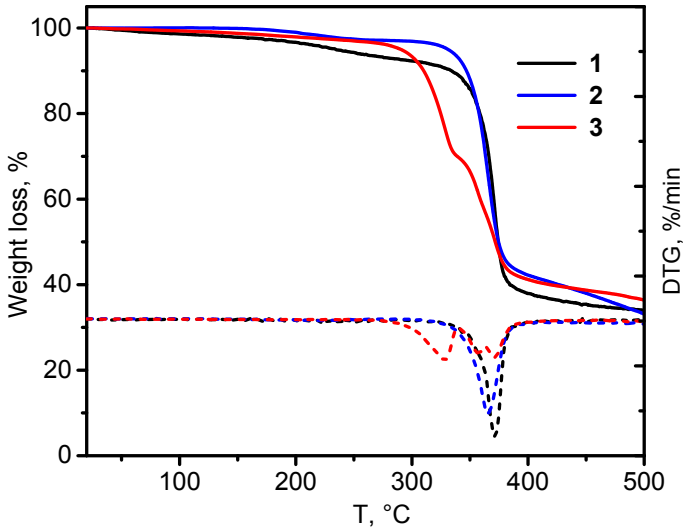

Figure S8. TGA&DTG curves for **1**–**3**.

§6. Computational details

The DFT calculations were made using the Amsterdam density functional[6–8] program with a gradient exchange functional GGA (BP86 – Becke[9] and Perdew[10,11]). Triple zeta basis sets, the “no frozen core” and scalar ZORA[12–15] approximations were used in all the calculations. Initial position of atoms is taken from X-

ray structure analysis. The geometry optimizations are made for dimers. Simulated IR spectra contained no imaginary frequencies. [16,17] Electronic excitation energies are found with Davidson's procedure for close-shell systems in a spin-restricted TDDFT calculation with scalar ZORA and no frozen core. [18]

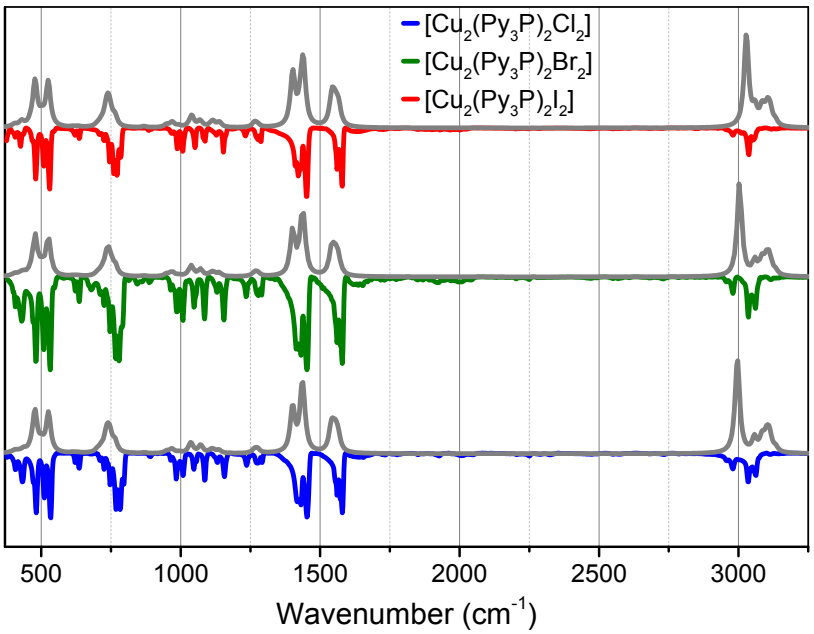

Figure S9. Experimental and computed (grey lines) IR spectra of **1**–**3**.

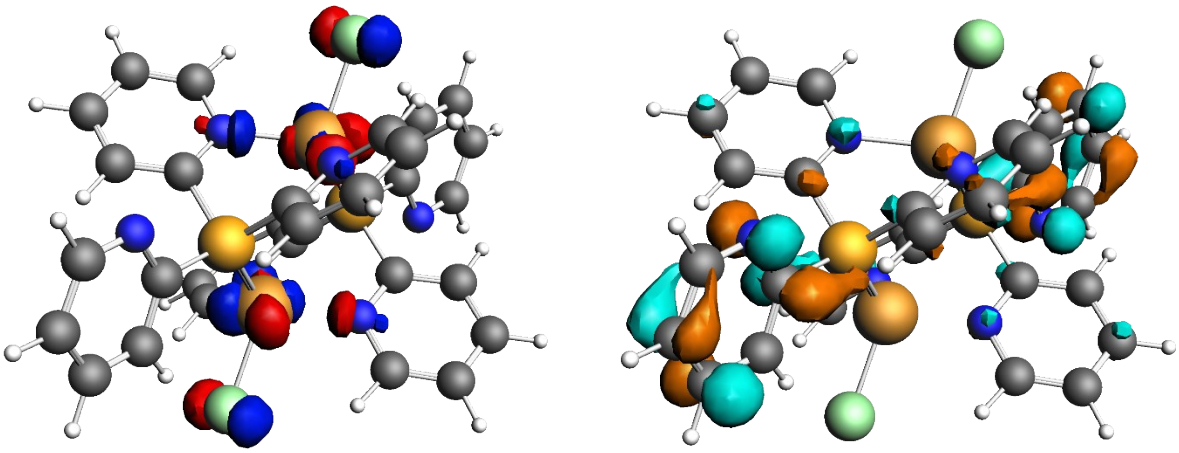

Figure S10. The HOMO (*left*) and LUMO diagrams for optimized **1** at the S_0 state.

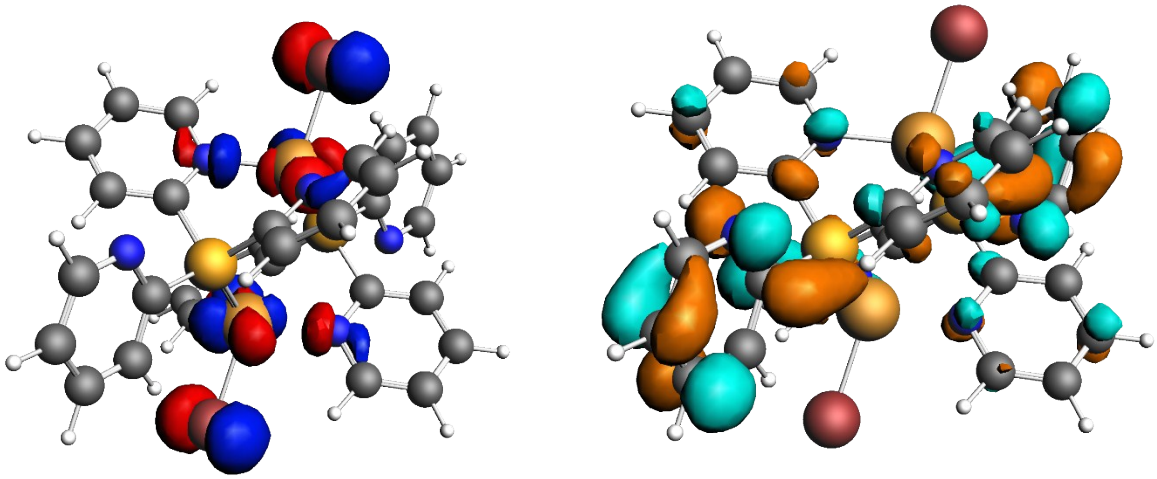

Figure S11. The HOMO (*left*) and LUMO diagrams for optimized **2** at the S_0 state.

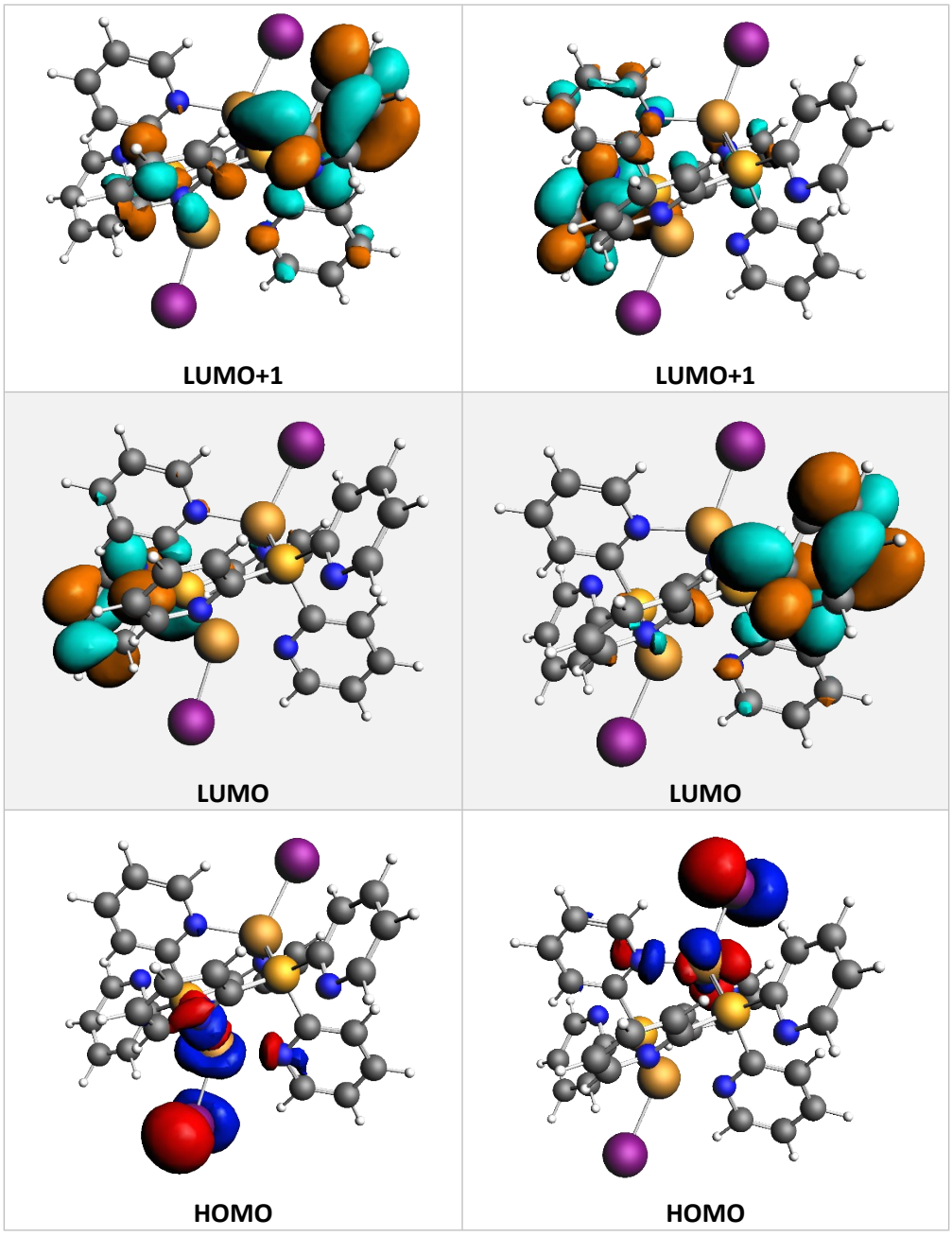

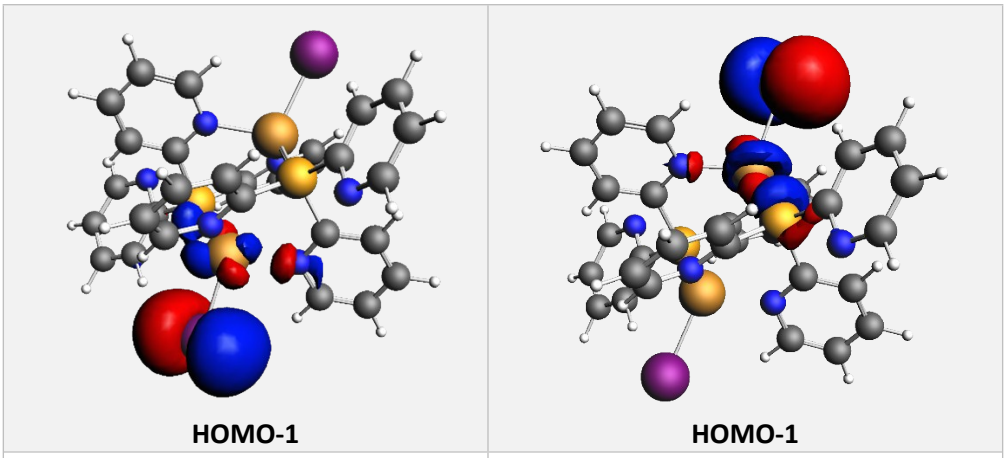

Figure S12. The frontier and near-frontier MOs for optimized S_1 (*left*) and T_1 states of **3**.

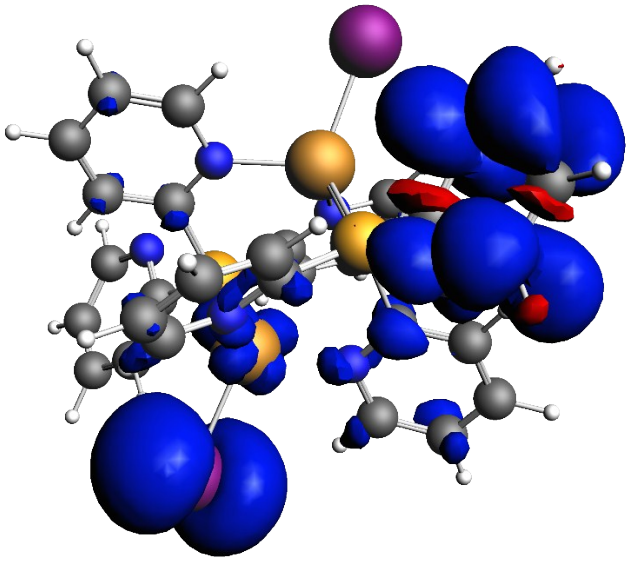

Figure S13. Spin density distribution in the T_1 state of **3** derived from DFT calculations.

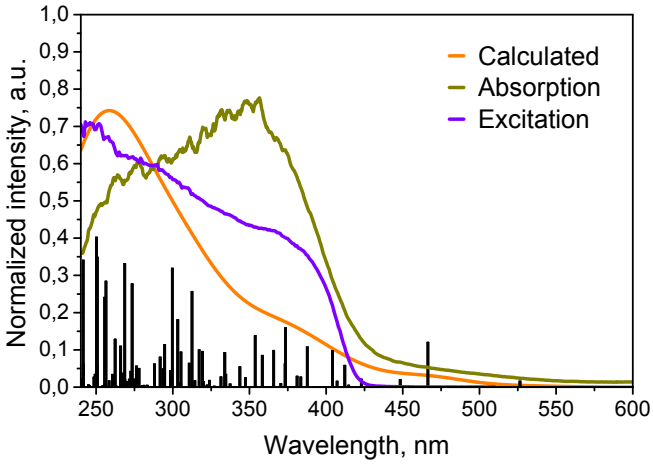

Figure S14. Comparison of the simulated UV-vis spectrum with experimental solid-state absorption and excitation ones of complex **1**. Vertical bars reflect the positions and oscillator strengths of the electronic transitions computed.

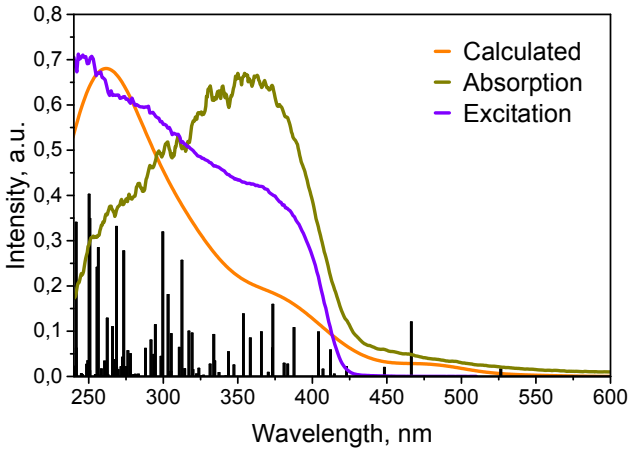

Figure S15. Comparison of the simulated UV-vis spectrum with experimental solid-state absorption and excitation ones for complex **2**. Vertical bars reflect the positions and oscillator strengths of the electronic transitions computed.

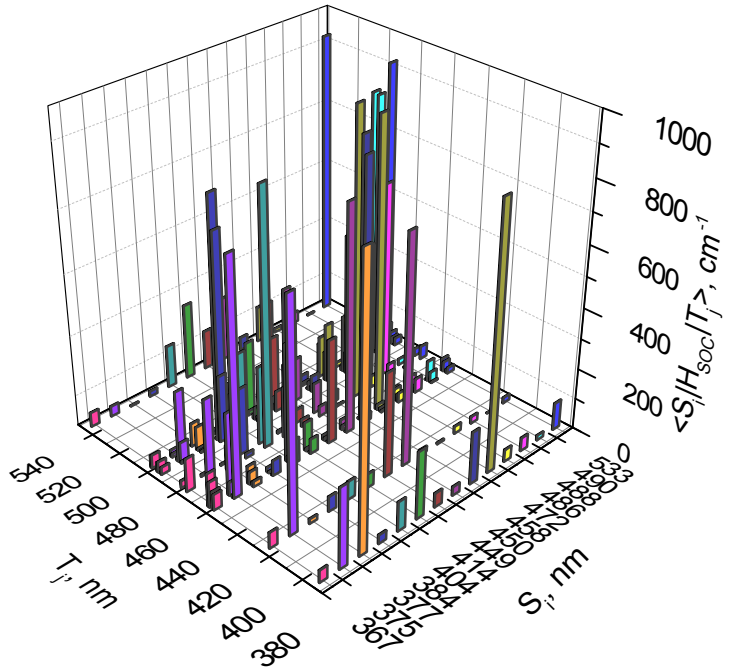

Figure S16. The SOC integrals (cm^{-1}) between different S_i (i = 1–14) and T_j (j = 1–15) states of **3**.

Table S2. Contribution of the atomic orbital to the molecular orbital for **1** in S_0 state according DFT.

	Contribution	Atomic orbital	Element
HOMO (-4.454 eV)	26.46%	d_{z2}	Cu
	21.79%	d_{x2-y2}	Cu
	10.93%	d_{yz}	Cu
	7.80%	p_x	Cl
	6.01%	p_x	N
	5.49%	p_z	N
	4.87%	p_z	Cl
	1.68%	s	N
	1.67%	d_{xy}	Cu

	1.67%	s	N
	1.20%	p_x	Cu
LUMO (-2.602 eV)	10.86%	p_x	C
	10.77%	p_x	N
	8.52%	p_x	C
	6.53%	p_x	C
	6.35%	p_z	C
	6.34%	p_z	N
	5.10%	p_z	C
	3.81%	p_z	C
	3.26%	p_x	P
	3.03%	p_y	C
	2.72%	p_z	N
	2.64%	p_z	C
	2.05%	p_x	C
	2.00%	p_z	P
	1.98%	p_z	C
	1.72%	p_x	C
	1.60%	p_y	C
	1.60%	p_x	N
	1.44%	p_y	N
	1.42%	p_z	C
	1.28%	p_x	C
	-1.25%	p_x	N
	1.21%	p_y	C
	1.20%	p_y	N
	1.10%	p_x	C
	1.09%	p_x	C
	1.02%	p_z	C

Table S3. Contribution of the atomic orbital to the molecular orbital for **2** in S_0 state according DFT.

	Contribution	Atomic orbital	Element
HOMO (-4.529 eV)	24.20%	d_{z2}	Cu
	20.14%	d_{x2-y2}	Cu
	11.56%	p_x	Br
	10.27%	d_{yz}	Cu
	7.30%	p_z	Br
	5.57%	p_x	N
	5.01%	p_z	N
	1.67%	d_{xy}	Cu
	1.54%	s	N
	1.52%	s	N
	1.13%	p_y	Br
	1.02%	p_x	Cu
LUMO (-2.657 eV)	10.61%	p_x	C
	10.55%	p_x	N
	8.29%	p_x	C
	6.35%	p_x	C

	6.28%	p_z	C
	6.28%	p_z	N
	4.99%	p_z	C
	3.75%	p_z	C
	3.36%	p_x	P
	3.22%	p_y	C
	2.80%	p_z	N
	2.72%	p_z	C
	2.18%	p_x	C
	2.08%	p_z	C
	2.05%	p_z	P
	1.73%	p_x	C
	1.72%	p_y	C
	1.65%	p_x	N
	1.59%	p_y	N
	1.53%	p_z	C
	1.33%	p_x	C
	1.14%	p_x	C
	1.08%	p_y	C
	1.08%	p_x	C
	1.07%	p_y	N
	1.03%	p_z	C

Table S4. Contribution of the atomic orbital to the molecular orbital for **3** in S_0 state according DFT.

	Contribution	Atomic orbital	Element
HOMO (-4.575 eV)	10.86%	p_x	I
	10.86%	p_x	I
	8.54%	d_{z2}	Cu
	8.54%	d_{z2}	Cu
	8.41%	d_{x2-y2}	Cu
	8.41%	d_{x2-y2}	Cu
	7.16%	p_z	I
	7.16%	p_z	I
	4.36%	d_{yz}	Cu
	4.36%	d_{yz}	Cu
	1.97%	p_x	N
	1.97%	p_x	N
	1.86%	p_y	I
	1.86%	p_y	I
	1.76%	p_z	N
	1.76%	p_z	N
LUMO (-2.738 eV)	4.87%	p_x	C
	4.87%	p_x	C
	4.84%	p_x	N
	4.84%	p_x	N
	3.74%	p_x	C
	3.74%	p_x	C
	3.01%	p_z	C

	3.01%	p_z	C
	2.99%	p_z	N
	2.99%	p_z	N
	2.85%	p_x	C
	2.85%	p_x	C
	2.31%	p_z	C
	2.31%	p_z	C
	1.86%	p_y	C
	1.86%	p_y	C
	1.76%	p_z	C
	1.76%	p_z	C
	1.65%	p_x	P
	1.65%	p_x	P
	1.50%	p_z	N
	1.50%	p_z	N
	1.45%	p_z	C
	1.45%	p_z	C
	1.10%	p_z	C
	1.10%	p_z	C
	1.07%	p_x	C
	1.07%	p_x	C
	1.02%	p_z	P
	1.02%	p_z	P
	1.01%	p_y	N
	1.01%	p_y	N

§7. Photophysical data

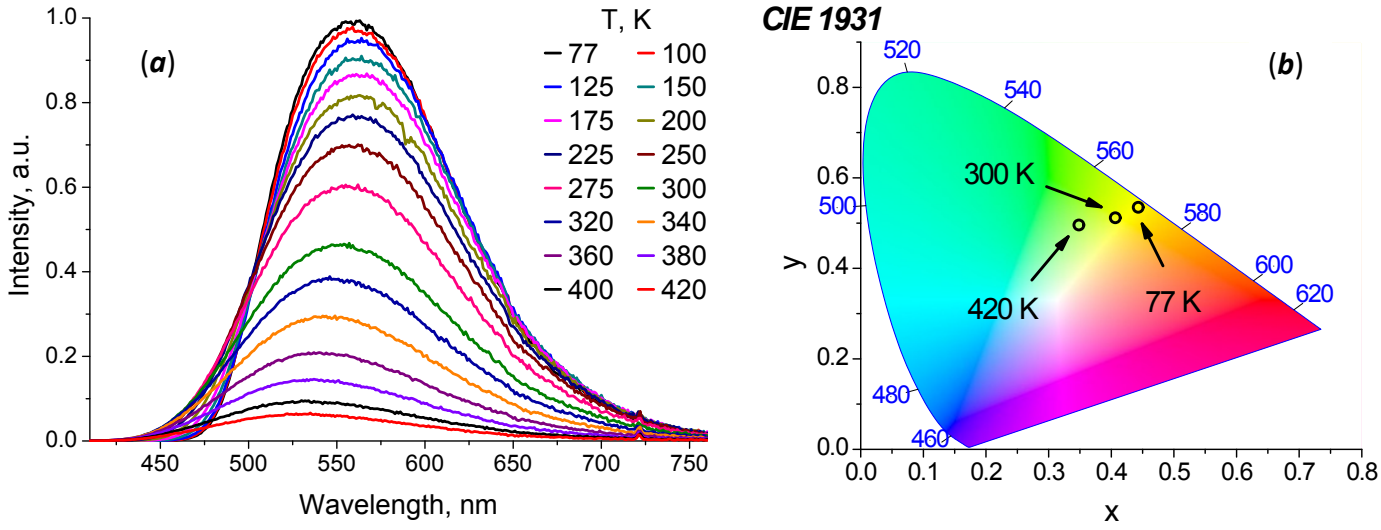

Figure S17. (***a***) Temperature-dependent emission spectra of **1** (λ_{ex} = 360 nm); (***b***) CIE 1931 diagram showing dynamics in photoluminescence chromaticity for solid **1** at the different temperatures.

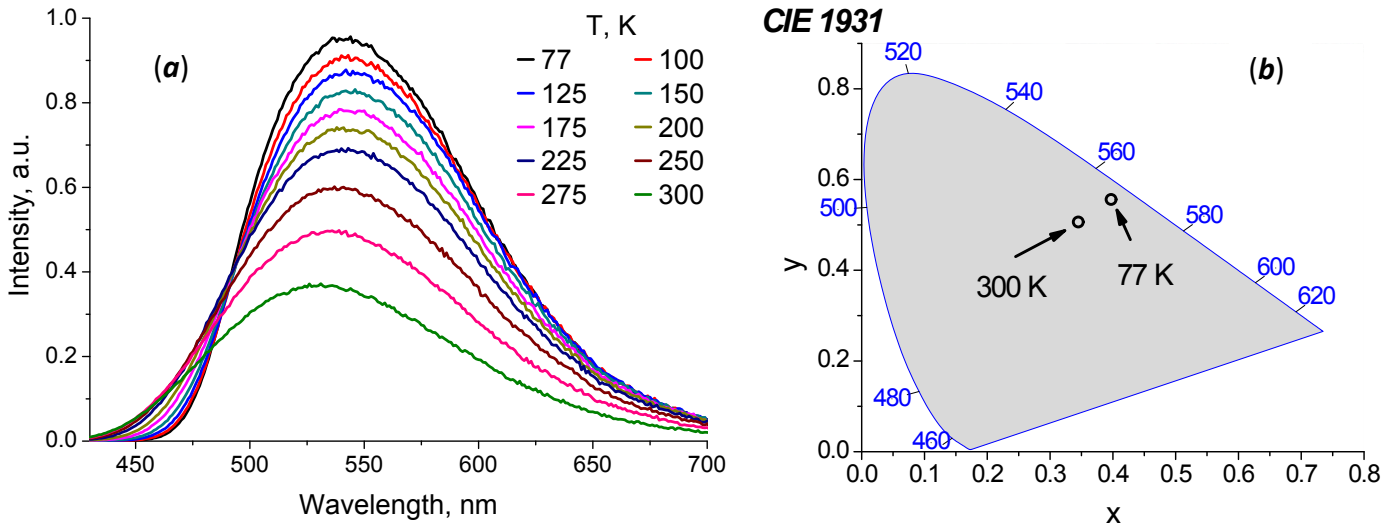

Figure S18. (***a***) Temperature-dependent emission spectra of **2** (λ_{ex} = 360 nm); (***b***) CIE 1931 diagram showing dynamics in photoluminescence chromaticity for solid **2** at the different temperatures.

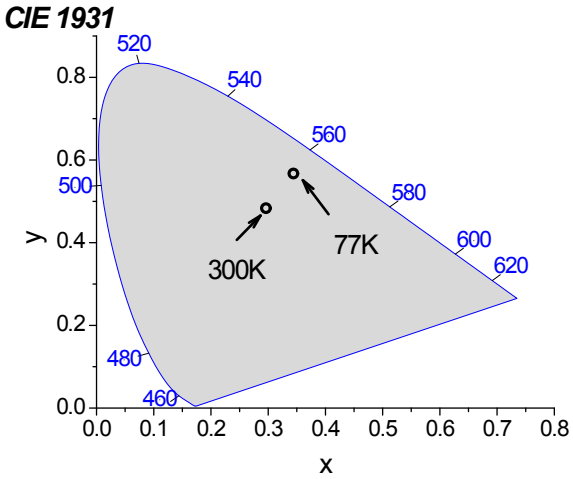

Figure S19. CIE 1931 diagram showing dynamics in photoluminescence chromaticity for solid **3** at the different temperatures.

*Gaussian analysis of the steady state and delayed emission spectra of **3***

The deconvolution of the steady state emission spectra of **3** has been carried out in the direct energy scale (eV) using the sum of two Gauss functions with the shared (but not fixed) E_{max} values of 2.275 eV (545 nm) and 2.463 eV (503 nm). The obtained superposition curves in the energy scale have been further converted into the wavelength scale (Figure S20).

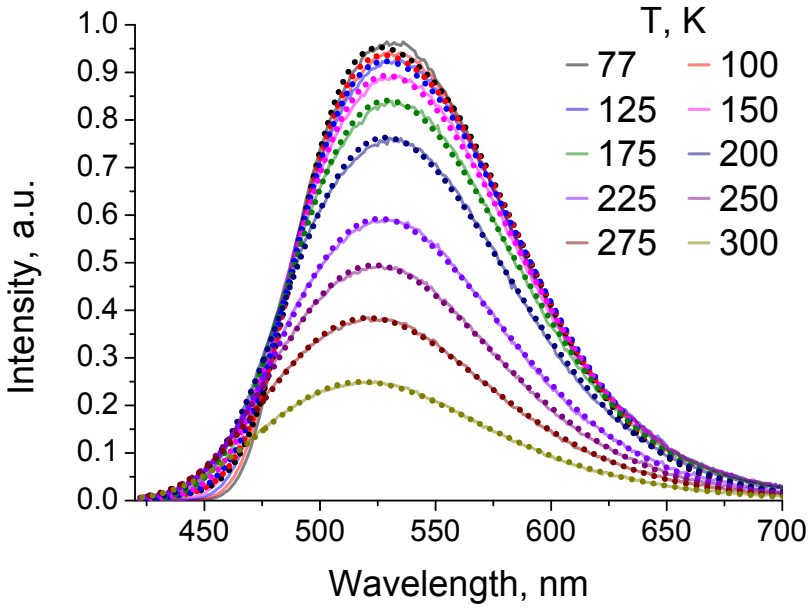

Figure S20. Deconvolution of the temperature dependence of the steady state PL spectra of **3** using two Gauss functions with shared E_{max} values of 2.275 eV (545 nm) and 2.463 eV (503 nm).

The same Gauss functions have also been exploited for fitting of the time-resolved PL spectra of **3** (Figure S21) on temperature range of 180–300 K, i.e. when the logarithmic value of the I_{TADF}/I_{PH} intensity relation is not tended to infinity.

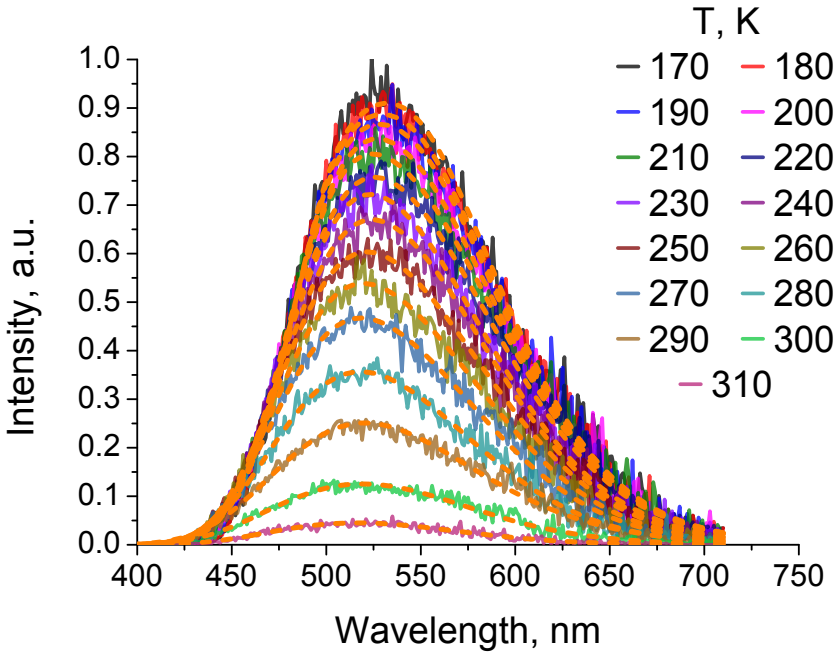

Figure S21. The time-resolved emission spectra of **3** fitted by two Gauss functions with shared E_{max} values of 545 nm and 503 nm (λ_{ex} = 360 nm, 50 μs delay).

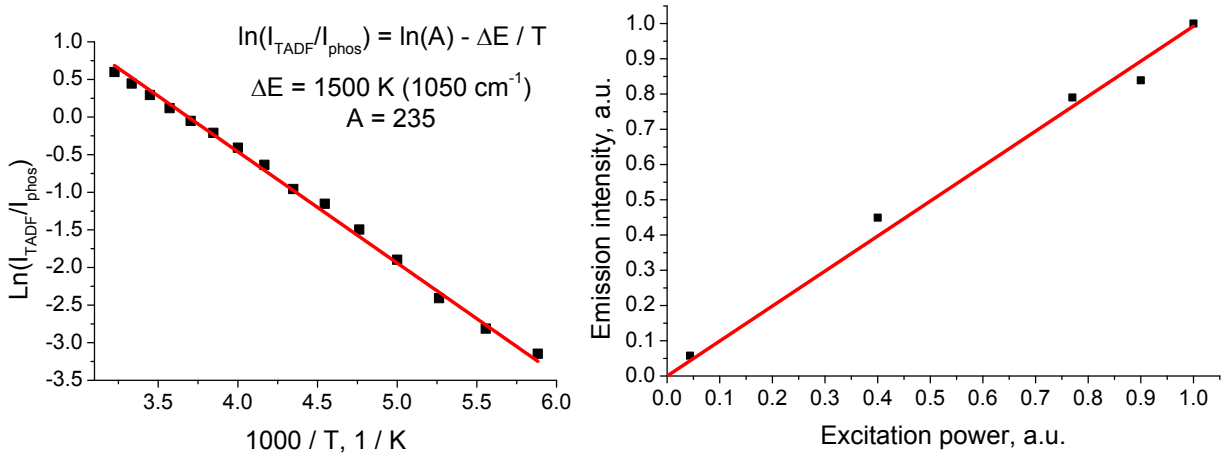

Figure S22. *Left*: Temperature dependence of the integral intensities ratio for the 503 nm band (I_{TADF}) and the 545 nm band (I_{phos}) of **3**, estimated by fitting of time-resolved emission spectra (Figure S21); *Right*: dependence of emission integral intensity of **3** on the excitation power at 300 K (λ_{ex} = 360 nm).

*Estimation of fractional contributions of TADF and phosphorescence to total emission of **1–3***

The relative contributions of phosphorescence (PH) and TADF in overall emission of **1–3** at a certain temperature have been estimated following the approach proposed by H. Yersin [ref. 27 and 29 in the main text]. Briefly, assuming that the quantum efficiencies of PH and TADF processes are close, the total rate constant of the luminescence, $k(T)$, can be written as a sum of the rate constants for both processes: $k(T) = k_{TADF}(T) + k_{PH} = \Phi_{PL}(T)/\tau(T)$. Since the τ/T curves of **1–3** reach a low-temperature below 125 K, the phosphorescence rate constants have been estimated following the equation: $k_{PH} = \Phi_{PL(77K)}/\tau_{77K}$. The TADF contribution at a certain temperature thus has been calculated using the equation: $k_{TADF}(T) = k(T) - k_{PH} = \Phi_{PL}(T)/\tau(T) - k_{PH}$."

Luminescent sensing of bases

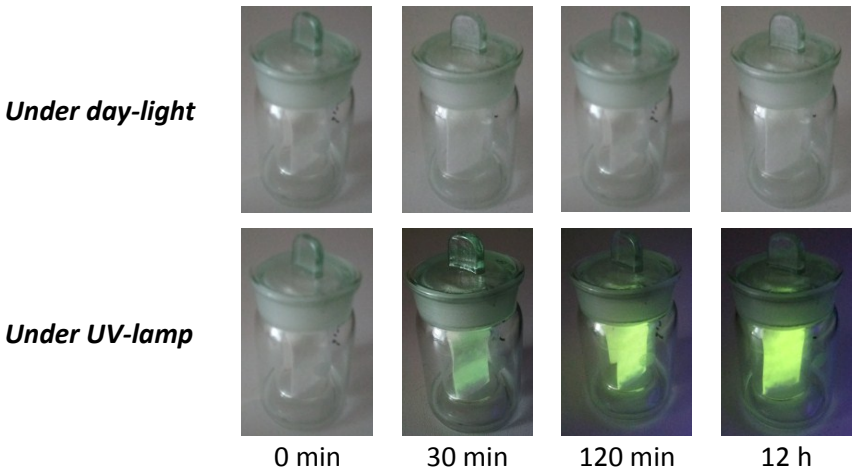

Figure S23. Dynamics of the luminescence enhancement associated with formation of the complex **1** during exposure of the paper, soaked in a HCl solution of **1**, under triethylamine vapors.

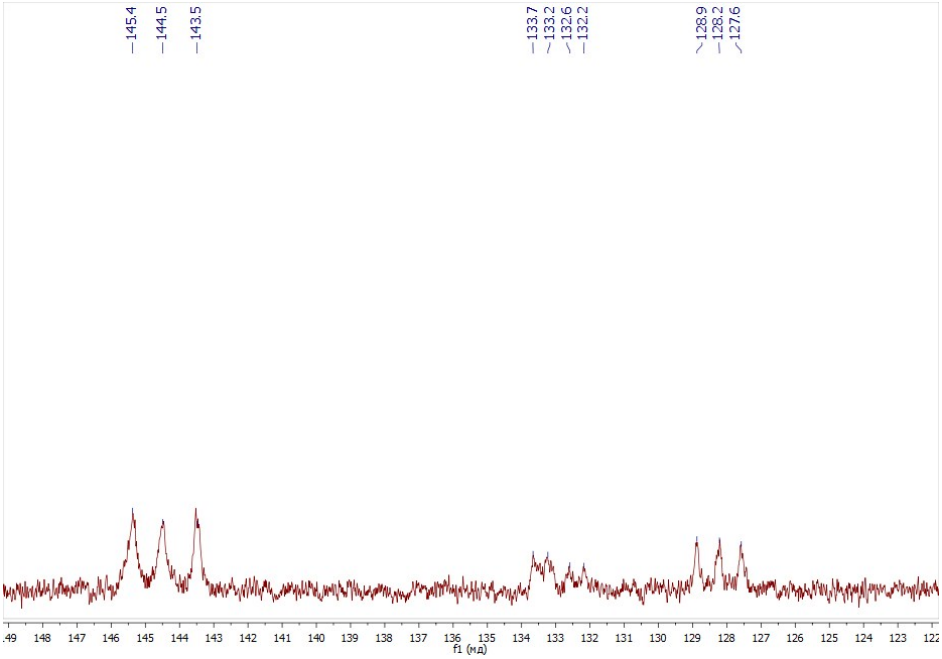

Figure S24. ^{13}C NMR spectrum of solution prepared by dissolution of **1** in hydrochloric acid (~30% in water).

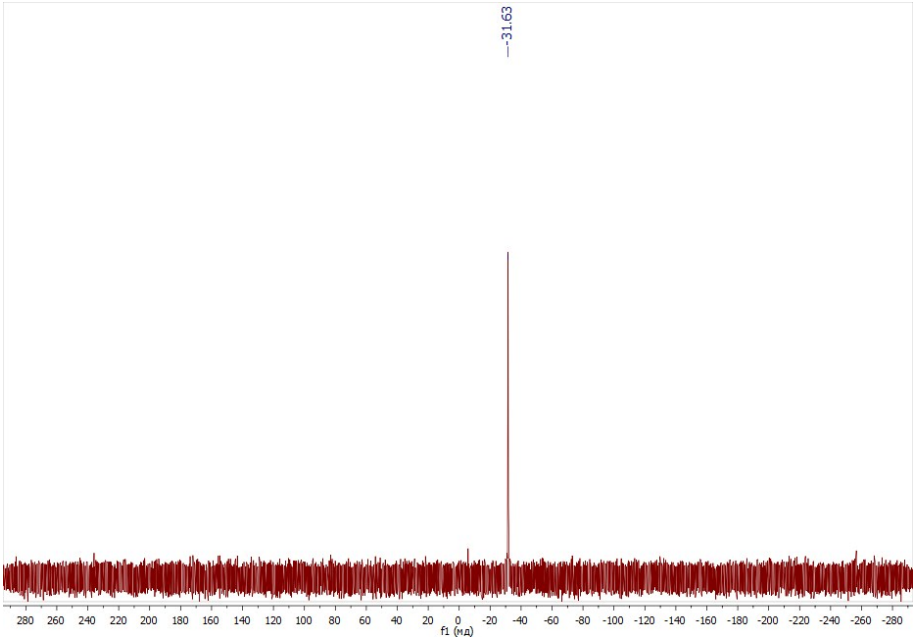

Figure S25. $^{31}P\{^{1}H\}$ NMR spectrum of solution prepared by dissolution of **1** in hydrochloric acid (~30% in water).

§8. References

[1] B. A. Trofimov, A. V. Artem'ev, S. F. Malysheva, N. K. Gusarova, N. A. Belogorlova, A. O. Korocheva, Yu. V. Gatilov and V. I. Mamatyuk, *Tetrahedron Lett*., 2012, **53**, 2424–2427.
[2] P. Bertani, J. Raya, B. Bechinger, *Solid State Nucl. Magn. Reson*., **2014**, *61–62*, 15–18.
[3] CrysAlisPro 1.171.38.46, *Rigaku Oxford Diffraction*, 2015.
[4] G. M. Sheldrick *Acta Crystallogr*., **2015**, *A71*, 3–8.
[5] G. M. Sheldrick, *Acta Crystallogr*., **2015**, *C71*, 3–8.
[6] G. te Velde, F. M. Bickelhaupt, E. J. Baerends, C. Fonseca Guerra, S. J. A. van Gisbergen, J. G. Snijders and T. Ziegler, Chemistry with ADF, *J. Comput. Chem.*, **2001**, *22*, 931.
[7] C. Fonseca Guerra, J. G. Snijders, G. te Velde and E. J. Baerends, *Theor. Chem. Acc.*, **1998**, *99*, 391.

[8] ADF2017, SCM, Theoretical Chemistry, Vrije Universiteit, Amsterdam, The Netherlands, http://www.scm.com.
[9] A. D. Becke, *Phys. Rev. A*, **1988**, *38*, 3098.
[10] J. P. Perdew, *Phys. Rev. B: Condens. Matter*, **1986**, *33*, 8822.
[11] Erratum: J. P. Perdew, *Phys. Rev. B: Condens. Matter*, **1986**, *34*, 7406.
[12] M. R. Pederson, S. N. Khanna, *Phys. Rev. B: Condens. Matter*, **1999**, *60*, 9566.
[13] F. Neese, *J. Chem. Phys.*, **2007**, *127*, 164112.
[14] C. van Wüllen, *J. Chem. Phys.*, **2009**, *130*, 194109.
[15] S. Schmitt, P. Jost, C. van Wüllen, *J. Chem. Phys.*, **2011**, *134*, 194113.
[16] L. Fan, T. Ziegler, *J. Chem. Phys.*, **1992**, *96*, 9005–9012.
[17] L. Fan, T. Ziegler, *J. Phys. Chem.*, **1992**, *96*, 6937–6941.
[18] S. J. A. van Gisbergen, J. G. Snijders, E. J. Baerends, *Comput. Phys. Commun.*, **1999**, *118*, 119.